



**CHALMERS**  
UNIVERSITY OF TECHNOLOGY

## **Modeling VOC-emissions in a building using Laplace networks – simplified models, explicit expressions and typical timescales**

Downloaded from: <https://research.chalmers.se>, 2026-05-16 15:07 UTC

Citation for the original published paper (version of record):

Domhagen, F., Hagentoft, C. (2025). Modeling VOC-emissions in a building using Laplace networks – simplified models, explicit expressions and typical timescales. *Indoor Environments*, 2(4).  
<http://dx.doi.org/10.1016/j.indenv.2025.100130>

N.B. When citing this work, cite the original published paper.



## Modeling VOC-emissions in a building using Laplace networks – simplified models, explicit expressions and typical timescales

Fredrik Domhagen<sup>\*</sup> , Carl-Eric Hagentoft

Department of Architecture and Civil Engineering, Chalmers University of Technology, Gothenburg SE-41296, Sweden

### ARTICLE INFO

#### Keywords:

VOC  
Diffusion  
Emission  
Ventilation threshold  
Ventilation  
Laplace networks

### ABSTRACT

New buildings often initially have elevated levels of VOC emissions that negatively affect the perceived indoor air quality. Increased ventilation is therefore commonly used in new buildings to reduce VOC concentrations and speed up the depletion of VOC within the materials. In this work we present a new analytic method, using Laplace networks, for precise prediction and analysis of VOC emissions in new buildings. The method handles multiple materials and is flexible and easily extendable to more complex cases. The method is validated with numerical simulations and used to analyze a room specific time-constant for assessing early-stage emissions. Results show that the time-constant, together with a general eefc-function, is useful for relating material properties, emitting area and ventilation rates to time. The proposed method is also used to derive several simplified models that predict emissions and concentrations at various stages, giving new insights into the impact from input parameters and relevant timescales. Given its high computational speed, the method is also proven to be suitable for uncertainty analysis when input data is limited.

### 1. Introduction

Volatile organic compounds (VOCs) are among the most prevalent pollutants found in the indoor air [1,2]. Occupants often detect VOCs as unpleasant odors, and exposure can negatively impact mental performance and productivity [3]. Examples of VOCs are formaldehyde, benzene, toluene, ethylbenzene and  $\alpha$ -pinene and major indoor sources are building materials, paints, solvents, wood preservatives and furnishing materials [4–6].

Furthermore, VOC levels not associated with occupants, which are emitted by materials, tend to be higher in newly constructed buildings and may take several months to decrease to acceptable levels [7]. This reduction follows a nonlinear pattern, influenced by both the diffusion of VOCs within materials and the ventilation of the room.

Prediction of VOC emissions from building materials is essential for improving indoor air quality and reducing the risk of unpleasant odors in the indoor environment, especially in new buildings. Predictive models can be categorized into two groups: non-physical models and physical models. Empirical models typically describe statistical regularities from measured data while physical models rely on valid mass-

transfer mechanisms and model parameters with well-defined physical meaning. Physical models are often preferred over non-physical models because of their transferability between different simulation conditions [8].

A common approach among the physical models is the  $c_0$ - $K_{ma}$ - $D_m$  models [9]. These models describe the diffusion of VOCs through a homogenous material, where  $D_m$  [ $m^2/s$ ] is the effective diffusion coefficient,  $K_{ma}$  [-] is a unitless partition coefficient that relates the concentration in the air-phase to the concentration in the sorbed-phase and  $c_0$  [ $kg/m^3$ ] is the initial concentration in the material.

With accurate enough input-data such physical models can predict VOC-concentrations in both field [10,11] and laboratory chamber tests [12]. If correctly implemented, any  $c_0$ - $K_{ma}$ - $D_m$  model with the same boundary conditions will yield the same results independent of the solution technique used. Thus, the accuracy of the model is dependent on the accuracy of the input data, typically determined from chamber measurements. The accuracy in those measurements is generally considered acceptable for engineering applications, for example, Xiong et al. reports a relative standard deviation for  $c_0$ ,  $K_{ma}$  and  $D_m$  that are all below 10 % using the C-history method [13,14].

<sup>\*</sup> Corresponding author.

E-mail address: [fredrik.domhagen@chalmers.se](mailto:fredrik.domhagen@chalmers.se) (F. Domhagen).

The  $c_0$ - $K_{ma}$ - $D_m$  models available in the literature today often lack flexibility with limitations regarding, for example, number of materials or zones that can be accounted for [8,11,18]. In fact, often these models are developed with the purpose of determining emission characteristics of building materials from chamber measurements and not for prediction of VOC-concentrations in more complex scenarios [13,19–22]. While numerical models can be built (as demonstrated later in this article) using, for example, MATLAB’s inbuilt ODE-solver, their drawback is long computation times and numerical stability. In contrast, analytical solutions are both faster, stable and provide useful information about the relation between input parameters. Thus, there is a need for a flexible method that can be used to model whole-house VOC-emissions and handle multiple building components consisting of several layers of emitting or absorbing materials.

Table 1 shows a selection of models found in the literature. All listed models are based on  $c_0$ - $K_{ma}$ - $D_m$  and predict VOC-emissions at varying building complexities (for example single or multiple emitting surfaces etc.). All the listed models account for both buffering capacity of room air and convective surface mass transfer at the material-air interfaces.

The objective of this study is to develop a flexible and straightforward method for making exact predictions of emissions and concentrations in a ventilated room with an arbitrary number of emitting and absorbing materials. This is done with the use of Laplace networks and conductance’s derived for mass diffusion of VOC in porous materials. The result is a fast and flexible method for VOC predictions that is easily extended to cover more complex cases (several rooms and materials) than those presented in this article. The model presented, using Laplace networks, is referred to as the *analytical model* from here on.

The concept of a *ventilation threshold* was introduced by Domhagen et al. [27] for assessing the need for enhanced ventilation in new buildings. The idea is that there is an upper limit for the ventilation rate at which emission outflow from materials stop increasing as the ventilation rate increases. Today, new buildings are often ventilated at high ventilation rates during the first year with the purpose of speeding up the depletion of VOC from materials. The ventilation threshold is therefore a useful concept for setting ventilation rates more efficiently. In this study we, in addition to the objective described above, also elaborate on the concept of the ventilation threshold and demonstrate how predictions can be made for complex cases using the proposed analytical model.

The analytical model presented in this article is a novel approach to predicting VOC emissions and concentrations in buildings. It relies on the established  $c_0$ - $K_{ma}$ - $D_m$  diffusion model and provides efficient, straightforward, and flexible technique for deriving case specific solutions. With this model several materials, building components and

**Table 1**  
Comparison between a selection of VOC models found in the literature.

Model	Multiple emitting surfaces	Multi-layered materials	Multiple zones	Analytical solution
Haghighat and Huang (2003) [23]		X		
L. Z. Zhang and J. L (2004) [24]	X	X		
Karlsson et al. (2005) [10]	X	X	X	
B. Deng et al. (2008) [25]	X			X
B. Deng et al. (2010) [26]		X		X
M. Guo et al. (2020) [11]	X			
Model presented in this article	X	X	X	X

rooms can be coupled and graphically represented in a Laplace network.

The outline of the article is as follows. In the next section, *Model Development*, we describe the analytical model with its governing equations and a complete expression for one ventilated room with an arbitrary number of emitting surfaces. Here, we also show how simplified solutions can be derived and we provide an analysis based on asymptotic behaviors. In the *Results and Discussion* section we use the model to make predictions on an office room and compare the results with a numerical solution. Here we also provide a more in-depth analysis of the relation between emission rates and ventilation. In the section *Future work* we give a brief idea of our future research plans and in the section *Conclusions* we summarize the main findings in the article.

## 2. Model development

The solution technique of periodic networks was developed by Jóhannesson [15,16] and used to model and optimize heat losses in buildings. The method is handy since heat flows are solved using graphical representations (thermal networks) from which expressions for heat flows are derived from established reduction rules. Periodic networks, as the name suggests, are designed to handle periodic variations. However, they can be easily converted into Laplace networks to handle step-changes in temperature (or concentrations) instead of periodic variations [17].

In this study the one-dimensional emission of VOC from any number of materials placed inside a ventilated room is of interest. Fig. 1 illustrates the problem with three emitting materials. The ventilation rate in the room is denoted  $R_a$  ( $m^3s^{-1}$ ). Each material, with its associated material properties, is indexed with the subscript ‘i’. The derived model accounts for mass diffusion within the material, near surface convection and buffering capacity of the room assuming air and VOC is perfectly mixed.

The partial differential equation for the linear mass diffusion (Fick’s second law) inside each material reads:

$$D_m \frac{\partial^2 c_m}{\partial x^2} = \frac{\partial c_m}{\partial t} \quad 0 \leq x \leq L \quad t \geq 0 \tag{1}$$

where  $D_m$  ( $m^2s^{-1}$ ) is the effective diffusion coefficient and  $c_m$  ( $kg\ m^{-3}$ ) is the VOC concentration in the material. The concentration of VOC in the material phase differs from the concentration in its air pores (air phase). However, it is assumed that equilibrium between the two phases is established instantaneously and can therefore be described with the dimensionless partition coefficient  $K_{ma}$  (–):

$$c_m = K_{ma} \cdot c_a \tag{2}$$

With no emission through the back of the material the boundary condition is:

$$D_m \frac{\partial c_m}{\partial x} \Big|_{x=0} = 0 \tag{3}$$

The mass balance across the material surface is described with a mixed boundary condition (Robin boundary) that couples the material

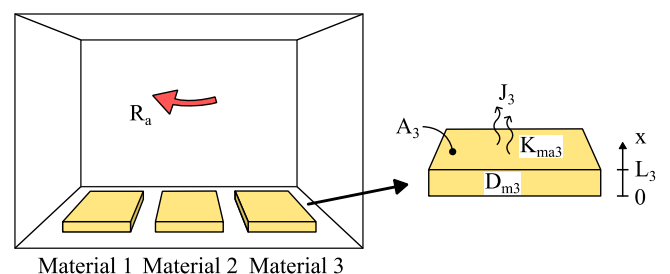


**Fig. 1.** Principle drawing of the model showing a ventilated room with three materials (either emitting, absorbing or both).

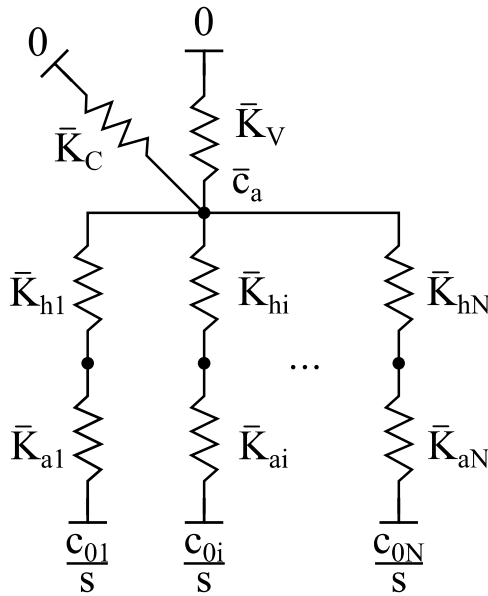


Fig. 2. Laplace network for a ventilated room with N number of emitting materials.

diffusion with convective mass transfer:

$$D_m \frac{\partial c_m}{\partial x} \Big|_{x=L} + h \cdot \left( \frac{c_m}{K_{ma}} \Big|_{x=L} - c_a \right) = 0 \quad (4)$$

where  $h$  ( $m s^{-1}$ ) is the convective mass transfer coefficient, and  $c_a$  ( $kg m^{-3}$ ) is the concentration in the air in the room. The mass balance for the ventilated room including the buffering capacity of its air volume,  $V$  ( $m^3$ ), is:

$$V \frac{\partial c_a}{\partial t} + c_a R_a - A h \cdot \left( \frac{c_m}{K_{ma}} \Big|_{x=L} - c_a \right) = 0 \quad (5)$$

The total rate of emission/absorption,  $J$  ( $kg s^{-1}$ ), across the material surface is given by the following expression:

$$J = -AD_m \frac{\partial c_m}{\partial x} \Big|_{x=L} \quad (6)$$

where  $A$  ( $m^2$ ) is the emitting or absorbing surface area.

### 2.1. Laplace networks – general solution

The expression for room concentration is derived using Laplace networks. This technique is closely related to periodic networks commonly used for analyzing periodically varying heat transfer in buildings. The advantage of the method is the possibility to systematically set up the periodic network and simplify it using established reduction rules. Such networks consist of temperature nodes connected by conductance's that describe heat transfer. For a more complete description the reader is referred to [28]. For a step-change at the boundaries, rather than periodic behavior, periodic networks can be easily converted to Laplace networks using the following substitution [17]:

$$\sqrt{\frac{2i\pi}{at_p}} \rightarrow \sqrt{\frac{s}{a}} \quad (7)$$

Using the analogies between heat- and mass transfer, relevant conductance's are, in this paper, defined from periodic conductance's and converted to the Laplace network. The network for the problem at hand,

depicted in Fig. 1, is shown in Fig. 2 where the initial concentration in the room and the exterior outdoor concentration is zero. Initial concentrations for the materials are here given in their air phase as described by Eq. (2).

The conductance for the buffering capacity of the air in the room:

$$\bar{K}_C = Vs \quad (8)$$

The conductance for the VOC transfer by ventilation:

$$\bar{K}_V = R_a \quad (9)$$

Conductance for convective surface transfer:

$$\bar{K}_{hi} = h_i A_i \quad (10)$$

The admittive conductance becomes:

$$\bar{K}_{ai} = R_a \tanh(L_i q_i) \frac{\sqrt{s}}{\beta_i} \quad (11)$$

where:

$$\beta_i = \frac{R_a}{K_{mai} \sqrt{D_{mi} A_i}} \quad (12)$$

$$q_i = \sqrt{\frac{s}{D_{mi}}} \quad (13)$$

The balance equation for the network described in Fig. 2 then becomes:

$$(0 - \bar{c}_a) \cdot \bar{K}_C + (0 - \bar{c}_a) \cdot \bar{K}_V + \sum_{i=1}^N \left( \frac{1}{s} \cdot c_{0i} - \bar{c}_a \right) \cdot \frac{\bar{K}_{ai} \bar{K}_{hi}}{\bar{K}_{ai} + \bar{K}_{hi}} = 0$$

$$\rightarrow \bar{c}_a(s) = \frac{\frac{1}{s} \sum_{i=1}^N c_{0i} \frac{\bar{K}_{ai} \bar{K}_{hi}}{\bar{K}_{ai} + \bar{K}_{hi}}}{\bar{K}_C + \bar{K}_V + \sum_{i=1}^N \frac{\bar{K}_{ai} \bar{K}_{hi}}{\bar{K}_{ai} + \bar{K}_{hi}}} \quad (14)$$

Substituting the expressions (8)-(11) gives the concentration in the room:

$$\bar{c}_a(s) = \frac{\frac{1}{s} \sum_{i=1}^N c_{0i} \frac{\sqrt{s} A_i h_i \tanh(L_i q_i)}{R_a \sqrt{s} \tanh(L_i q_i) + \beta_i A_i h_i}}{1 + \frac{Vs}{R_a} + \sum_{i=1}^N \frac{\sqrt{s} A_i h_i \tanh(L_i q_i)}{R_a \sqrt{s} \tanh(L_i q_i) + \beta_i A_i h_i}} \quad (15)$$

The total emission/absorption for one surface:

$$\bar{J}_i = \frac{R_a \sqrt{s} \tanh(L_i q_i) A_i h_i}{R_a \sqrt{s} \tanh(L_i q_i) + \beta_i A_i h_i} \cdot \left( \frac{c_{0i}}{s} - \bar{c}_a(s) \right) \quad (16)$$

And the total emission from all surfaces:

$$\bar{J} = \sum_{i=1}^N \bar{J}_i \quad (17)$$

Note that these expressions give room concentrations and emission rates for a ventilated room with any number of single-layered materials with a perfectly tight backside, accounting for surface convection and room buffering capacity. The expressions are given in the Laplace domain and are not easily inverted analytically or explicitly. Fortunately, there are a vast number of algorithms for numerical inversion of Laplace transforms that can be used [29]. Inversion algorithms based on Fourier-series are considered economical and robust with respect to free parameters [30]. For inverting the expressions derived in this study, we found the Fourier-series based algorithm by de Hoog's [31] to be robust and reliable. In addition, implementations of the algorithm are readily available in the python package mpmath [32] and MATLAB [33]. For the analysis in this study, we use MATLAB. In the section Comparison

with numerical solution below, the accuracy of the algorithm is compared with a conventional numerical solution.

## 2.2. Simplified solutions

The expression, Eq. (15), can be simplified by neglecting surface convection resistance and the buffering capacity in the room and assuming that materials can be regarded as semi-infinite (valid for short times where  $t < L^2/D_m$ ):

$$\bar{c}_a(s) = \frac{1}{s} \frac{\sum_{i=1}^N c_{0i} \frac{\sqrt{s} A_i h_i \tanh(L_i q_i)}{R_a \sqrt{s} \tanh(L_i q_i) + \beta_i A_i h_i}}{1 + \frac{Vs}{R_a} + \sum_{i=1}^N \frac{\sqrt{s} A_i h_i \tanh(L_i q_i)}{R_a \sqrt{s} \tanh(L_i q_i) + \beta_i A_i h_i}} \rightarrow \frac{1}{s} \frac{\sum_{i=1}^N \frac{c_{0i}}{\beta_i}}{\frac{1}{\sqrt{s}} + \sum_{i=1}^N \frac{1}{\beta_i}} \quad (18)$$

The expression is inverted using standard tables of Laplace transforms:

$$c_a(t) = \left( \frac{\frac{c_{01}}{\beta_1} + \frac{c_{02}}{\beta_2} + \dots + \frac{c_{0N}}{\beta_N}}{\sum_{i=1}^N \frac{1}{\beta_i}} \right) \exp\left(-\frac{t}{\left(\sum_{i=1}^N \frac{1}{\beta_i}\right)^2}\right) \operatorname{erfc}\left(\frac{\sqrt{t}}{\sum_{i=1}^N \frac{1}{\beta_i}}\right) \quad (19)$$

With the introduction of a time-constant:

$$t_c = \left(\sum_{i=1}^N \frac{1}{\beta_i}\right)^2 = \frac{1}{R_a^2} \left(\sum_{i=1}^N K_{mai} \sqrt{D_{mi}} A_i\right)^2 \quad (20)$$

Eq. (19) can be expressed in a more compact form:

$$c_a(t) = c_0 \cdot \operatorname{erfc}\left(\sqrt{\frac{t}{t_c}}\right) \quad (21)$$

$$\operatorname{erfc}\left(\sqrt{\phi}\right) = \exp(\phi) \operatorname{erfc}\left(\sqrt{\phi}\right)$$

$$c_0 = \frac{\frac{c_{01}}{\beta_1} + \frac{c_{02}}{\beta_2} + \dots + \frac{c_{0N}}{\beta_N}}{\sum_{i=1}^N \frac{1}{\beta_i}} = \frac{\sum_{i=1}^N c_{0i} \cdot K_{mai} \sqrt{D_{mi}} A_i}{\sum_{j=1}^N K_{maj} \sqrt{D_{mj}} A_j}$$

The last term, from heron named the  $\operatorname{erfc}$ -function, is unitless and describes how the concentration changes over time. The preceding term, denoted  $c_0$ , is the indoor concentration at time zero. It consists of the sum of the initial concentration for each material weighed by its respective  $\beta = R_a/K_{mai} \sqrt{D_{mi}} A_i$ . A higher  $\beta$  for a material means that its initial concentration is less influential on the total initial concentration.

The above expression is useful for analyzing the contribution of one of the materials to the total concentration in the room. For example, the contribution for one material to the room concentration:

$$c_j(t) = \frac{c_{0j} \frac{1}{\beta_j}}{\sum_{i=1}^N \frac{1}{\beta_i}} \exp\left(-\frac{t}{t_c}\right) \operatorname{erfc}\left(\sqrt{\frac{t}{t_c}}\right) = \frac{c_{0j} \frac{1}{\beta_j}}{\sum_{i=1}^N \frac{1}{\beta_i}} \operatorname{erfc}\left(\sqrt{\frac{t}{t_c}}\right) \quad (22)$$

The concentration in the room is given by the sum of the contributions from all materials:

$$c_a(t) = \sum_{j=1}^N c_j(t) \quad (23)$$

Similarly, the emissions in the room with several materials, neglecting surface resistances, buffering capacity and assuming that the materials can be regarded as semi-infinite (combining Eqs. (15) and (16)):

$$\begin{cases} h \rightarrow \infty \\ V \rightarrow 0 \\ L \rightarrow \infty \end{cases}$$

$$\bar{J}_i = \frac{1}{s} \frac{R_a \sqrt{s} \tanh(L_i q_i) A_i h_i}{R_a \sqrt{s} \tanh(L_i q_i) + \beta_i A_i h_i} \cdot \left( c_{0i} - \frac{\sum_{j=1}^N c_{0j} \frac{\sqrt{s} \tanh(L_j q_j) A_j h_j}{R_a \sqrt{s} \tanh(L_j q_j) + \beta_j A_j h_j}}{1 + \frac{Vs}{R_a} + \sum_{j=1}^N \frac{\sqrt{s} \tanh(L_j q_j) A_j h_j}{R_a \sqrt{s} \tanh(L_j q_j) + \beta_j A_j h_j}} \right) \rightarrow \frac{1}{\sqrt{s}} \frac{R_a}{\beta_i} \cdot \left( c_{0i} - \frac{\sqrt{s} \cdot \sum_{j=1}^N c_{0j} \frac{1}{\beta_j}}{1 + \sqrt{s} \cdot \sum_{j=1}^N \frac{1}{\beta_j}} \right) \quad (24)$$

The emission rate for one material is the inverse Laplace transform of the above expression:

$$J_j(t) = \frac{R_a}{\beta_j} \left( \frac{c_{0j}}{\sqrt{\pi t}} - \frac{c_0}{t_c} \left( \sqrt{\frac{t}{t_c}} - \operatorname{erfc}\left(\sqrt{\frac{t}{t_c}}\right) \right) \right) \quad (25)$$

and the total emission rate from all the materials is given by:

$$J(t) = J_0 \cdot \operatorname{erfc}\left(\sqrt{\frac{t}{t_c}}\right) \quad (26)$$

$$J_0 = R_a \frac{\sum_{i=1}^N c_{0i}}{\sum_{i=1}^N \frac{1}{\beta_i}} = R_a \cdot c_0$$

This expression is similar to Eq. (21). The first part of the expression,  $J_0$ , is the total emission rate at time zero (compare with total initial concentration in Eq. (21)). The second part of the expression, the  $\operatorname{erfc}$ -function, is unitless and here it describes the change in emission rate over time. Note that Eq. (26) is equivalent to the expression derived in Domhagen et al. [27] with the exception that here the expression is extended to include several materials.

Both Eqs. (21) and (26) are based on a, time independent, initial term,  $c_0$  or  $J_0$ . These initial terms are calculated as superposed initial conditions for each material in the room and weighted based on the material properties for each material given by its respective  $\beta$ .

The expressions for the initial concentrations are useful for assessing the impact of each material and their early emissions. For example, it can be directly understood from these expressions that if two identical particle boards are placed in a room where one contains and emits VOC while the other is empty the early concentrations will be halved compared to if only one emitting particle board is put inside the room (assuming that the room buffering capacity is negligible).

$$c_0 = \frac{1}{\sum_{i=1}^2 \frac{1}{\beta_i}} \left( \frac{c_{01}}{\beta_1} + \frac{c_{02}}{\beta_2} \right) = \frac{\frac{c_{01}}{\beta} + \frac{0}{\beta}}{\frac{1}{\beta} + \frac{1}{\beta}} = \frac{c_{01}}{2} \quad \beta = \beta_1 = \beta_2 \quad (27)$$

The  $\operatorname{erfc}$ -function shows the decline of the emission concentration in the air, from the initial value of  $c_0$  down to zero. The argument,  $t/t_c$ , shows the crucial importance of the time scale  $t_c$ , determining the pace of the decline. As shown in Eq. (20), the time scale depends on ventilation rate, emitting area, partition coefficient and the diffusion coefficient.

Here we present another simplified solution where surface convection resistance is neglected while assuming that materials can be regarded as semi-infinite:

$$\bar{c}_a(s) = \frac{1}{s} \frac{\sum_{i=1}^N c_{0i} \frac{\sqrt{s} A_i h_i \tanh(L_i q_i)}{R_a \sqrt{s} \tanh(L_i q_i) + \beta_i A_i h_i}}{1 + \frac{Vs}{R_a} + \sum_{i=1}^N \frac{\sqrt{s} A_i h_i \tanh(L_i q_i)}{R_a \sqrt{s} \tanh(L_i q_i) + \beta_i A_i h_i}} \rightarrow \frac{\sum_{i=1}^N c_{0i}}{\sum_{i=1}^N \beta_i} \frac{1}{\sqrt{s}} \frac{\sum_{i=1}^N \frac{1}{\beta_i}}{1 + \frac{V}{R_a} s + \sqrt{s} \sum_{i=1}^N \frac{1}{\beta_i}}$$

$$= c_0 \frac{\frac{1}{\sqrt{s}} \sum_{i=1}^N \frac{1}{\beta_i}}{1 + \frac{V}{R_a} s + \sqrt{s} \sum_{i=1}^N \frac{1}{\beta_i}} \quad (28)$$

The solution is found by inversion of above the above expression:

$$c(t) = c_0 \frac{2}{\pi} \int_0^\infty \frac{(1 - \eta x^2)}{(1 - \eta x^2)^2 + x^2} \exp\left(-x^2 \frac{t}{t_c}\right) dx \quad (29)$$

Where  $\eta$  is a unitless parameter:

$$\eta = \frac{V/R_a}{t_c} \quad (30)$$

Here,  $\eta$  gives the relation between the time-scale related to the buffering capacity of the room air and the time-scale for the material emissions described by  $t_c$ . A higher  $\eta$  means that the buffering capacity is affecting the room concentration for a longer period of time during the initial phase of the emission process.

### 2.3. Approximations and asymptotic behavior for a room with one emitting surface

Fig. 3 shows the concentration of emission in the room air for an example with one emitting slab calculated using numerical inversion of the Laplace transform, Eq. (15). In this example the room air volume is 80 m<sup>3</sup>, the air exchange rate (ACH) is 0.5 h<sup>-1</sup>. The emitting surface is 100 m<sup>2</sup> and the thickness of the emitting material is 0.01 m. The diffusion coefficient is  $D_m = 5 \cdot 10^{-10} \text{m}^2 \text{s}^{-1}$ , partition coefficient is  $K_{ma} = 100$ , and surface resistance is  $h = 5 \cdot 10^{-4} \text{ms}^{-1}$ . These properties are estimated based on typical values found in the literature.

We can see an initial phase when the room air concentration is building up to a maximum whereafter the concentration is declining. In the very first phase the concentration of VOC is homogeneous in the slab at its initial concentration. The surface concentration is at its highest whereafter it is declining, thus emitting less VOC to the room air. The emission to the room air makes the concentration in the room air rise. The outflow of VOC from the room, due to the ventilation, reduces the

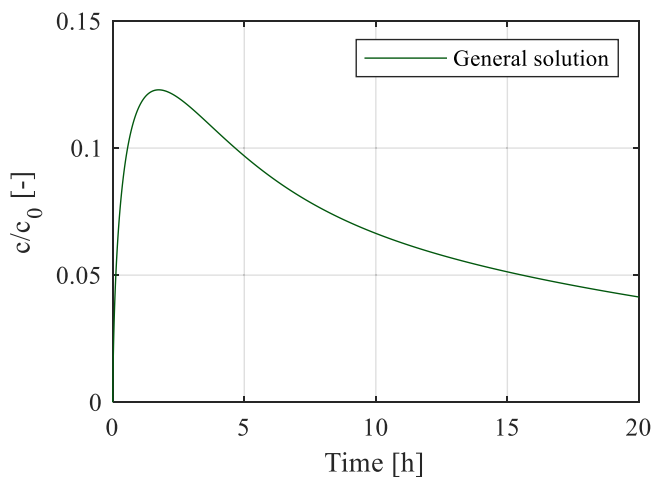


Fig. 3. Concentration in the room obtained from the general solution.

build-up but is small in the beginning and increases with time. For longer times both the emissions from the slab to the room and the flow of emissions out from the room due to the ventilation diminish.

The approximation of the room air concentration for small times can be obtained from an analysis using the Laplace expression, Eq. (15), with  $L = \infty$  and the frequency parameter  $s$  tending to infinity ( $s \rightarrow \infty$ ):

$$c_a(t) = c_0 \frac{A}{V} \frac{(K_{ma} \sqrt{D_m})^2}{h} \left( \text{erfc}\left(\sqrt{\frac{t}{t_0}}\right) - 1 + \frac{2}{\sqrt{\pi}} \sqrt{\frac{t}{t_0}} \right) \quad (31)$$

$$t_0 = \left( \frac{K_{ma} \sqrt{D_m}}{h} \right)^2$$

Fig. 4 shows the approximation, Eq. (31), for our example. The time parameter  $t_0$  is only 20 s so the first build-up period is very rapid.

Since the influence of the storage capacity of the room air decrease as time passes, the solution, Eq. (23), for the case of  $V \rightarrow 0$ ,  $L \rightarrow \infty$  and  $h \rightarrow \infty$ , is useful to understand the process and how the room concentration changes with time. The solution for our example is shown in Fig. 5. Here, the time parameter  $t_c$  is 405 s or 0.11 h. At this time,  $t = t_c$ , air concentration is reduced to 43 % of the initial concentration in the material pores. After 3.35 h, or  $20.9 \cdot t_c$ , the orange curve intersects the general solution (green curve). After some time, the concentration is over-estimated when using the simplified solution. This can be explained by the fact that the slab thickness is assumed to be infinite and with no surface resistance, thus the slab is never completely depleted and continues to supply VOC to the room indefinitely.

One important phase of the emission process is apparently when the emission releasing front hits the tight back side of the slab. The time,  $t_L$ , at which this happens can be approximated, using the heat analogy solutions:

$$\sqrt{D_m t_L} = L \quad t_L = \frac{L^2}{D_m} \quad (32)$$

In our example the time  $t_L$  is 55 h which is in the same order of magnitude as the time as shown in Fig. 5, which is around 20–30 h when the orange curve shows higher values.

For longer times, the room air capacity can be neglected. Using the heat analogy [28], with analytical solutions for the symmetrical case of temperature decline in a slab with thickness  $2L$  and a surface transport coefficient,  $h_{eq}$ , on both sides equal to:

$$h_{eq} = h \frac{1}{1 + \frac{Ah}{R_a}} \quad (33)$$

The analytical solution is expressed as an infinite sum with exponentially declining terms:

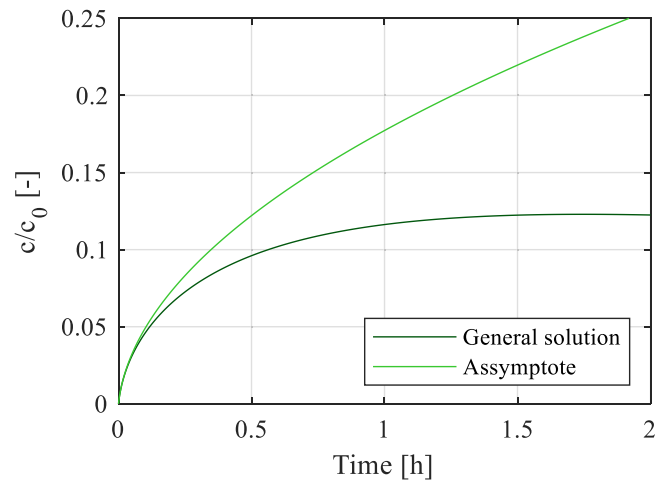


Fig. 4. Concentration in the room, obtained from the general solution together with the asymptote for small times.

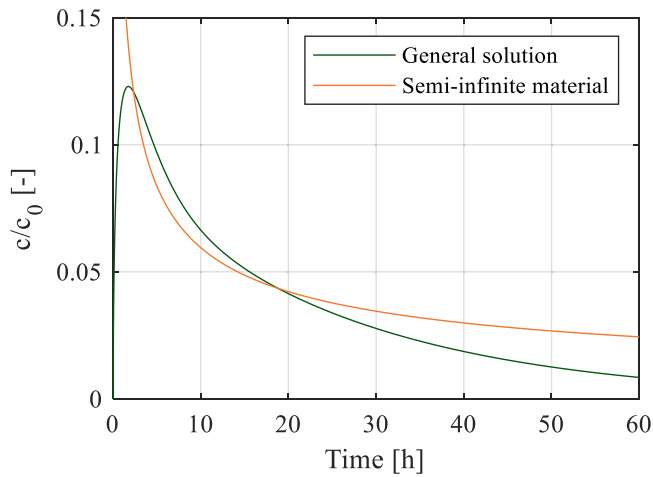


Fig. 5. Concentration in the room obtained from the general solution together with corresponding solution for a semi-infinite material.

$$J(t) = c_0 A D_m K_{ma} \frac{2L}{d^2} \sum_{n=1}^{\infty} \frac{1}{\left(1 + \frac{L}{d}\right) + b_n^2} \exp\left(-b_n^2 \frac{D_m t}{L^2}\right) \quad (34)$$

Where  $b_n$  are transcendental roots of:

$$b_n \tan(b_n) = \frac{L}{d} \quad (35)$$

and  $d$  is the equivalent thickness of the material in terms of convective mass transfer:

$$d = \frac{K_{ma} D_m}{h_{eq}} = \frac{K_{ma} D_m}{h} \left(1 + \frac{Ah}{R_a}\right) \quad (36)$$

When  $d$  is small in comparison with the material thickness Eq. (34) can be simplified to:

$$J(t) = c_0 A D_m K_{ma} \frac{2}{L} \sum_{n=1}^{\infty} \exp\left(-b_n^2 \frac{D_m t}{L^2}\right) \quad (37)$$

and the concentration in the room:

$$c(t) = \frac{J(t)}{R_a} \quad (38)$$

Fig. 6 shows the results for the example room presented above. Since

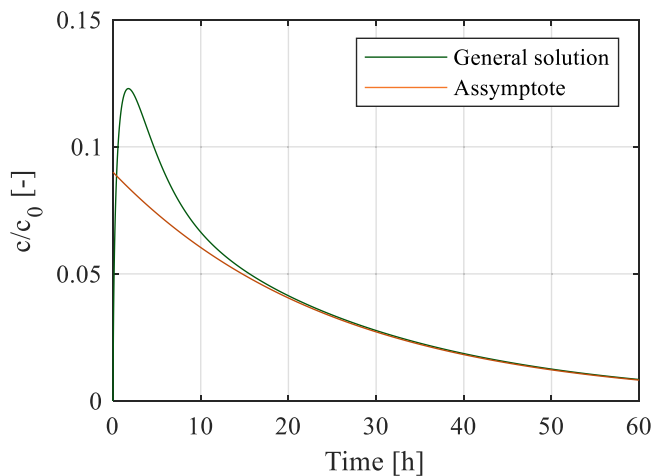


Fig. 6. Concentration in the room, obtained from the general solution together with the solution for long times.

we are only interested in the decline for longer times, only the first term in Eq. (37) is used. For times greater than 20 h the approximate solution matches the general solution, accounting for the limited thickness of the panel and the surface resistance.

To complete the lineup of approximations, there is also one for small times ( $L = \infty$ ), neglecting room air capacity ( $V = 0$ ) but accounting for the surface resistance,  $h$ . Once again, we can use the analogy with heat transfer in a semi-infinite slab:

$$\frac{c_a(t)}{c_0} = \frac{1}{1 + \frac{R_a}{Ah}} \operatorname{erfc}\left(\sqrt{\frac{t}{t_{c,h}}}\right) \quad (39)$$

$$t_{c,h} = t_c \cdot \left(1 + \frac{R_a}{Ah}\right)^2$$

Here, we see that the magnitude and the timescale are slightly different than for the case with  $h = \infty$ . In our example, the magnitude is reduced to 82 % and the time scale is increased by 49 %. The surface resistance is causing the magnitude to be slightly less, but the increased time scale makes it take longer for the room concentration to decline. In our example the difference in concentration with or without surface resistance is visible only during the first 3 h.

The impact that the room buffering capacity has on room concentration can be investigated using Eq. (29). Again, we will use the simplified example case with one emitting material. The results from the simulations can be seen in Fig. 7 where room concentrations are simulated at five different values of  $\eta$ . Here,  $\eta = 18$  is the reference case calculated from a room air volume of  $80 \text{ m}^3$ . The case with  $\eta = 0$  means that the buffering capacity is completely neglected, and the resulting concentration becomes the same as if using Eq. (21). As shown in Fig. 7 the effect of the buffering capacity on the room air concentration is significant only initially at timescales of a couple of hours. Note that in this example, the air exchange rate (ACH) is  $0.5 \text{ h}^{-1}$  which is typically considered to be at the lower end. For ventilation rates higher than this  $\eta$  will become smaller and consequently the effect of the room buffering capacity will be less significant.

#### 2.4. VOC depletion and ventilation

Air-flush is a strategy that is sometimes used to reduce early emissions in new buildings by increasing the ventilation rate for some time to speed up depletion of emissions [34]. The effect of ventilation on the emission rate is exemplified here with the example room presented in the previous section (one emitting material). The results from the simulations, using Eq. (16), are shown in Fig. 8. Here, we see that after 5 h

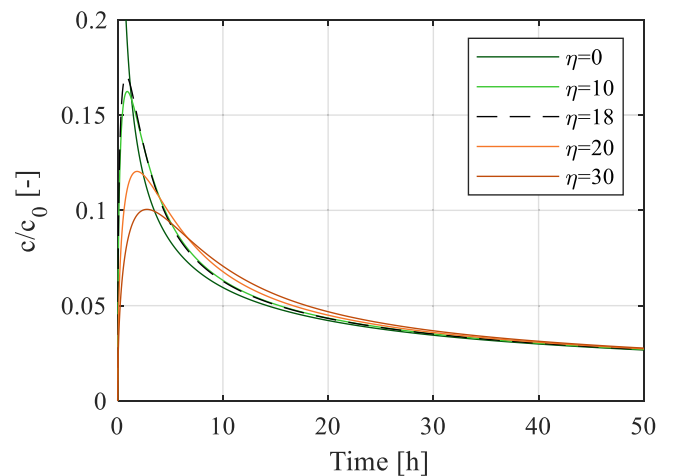


Fig. 7. The room air concentration with emission from one material at five distinct levels of room buffering capacity.

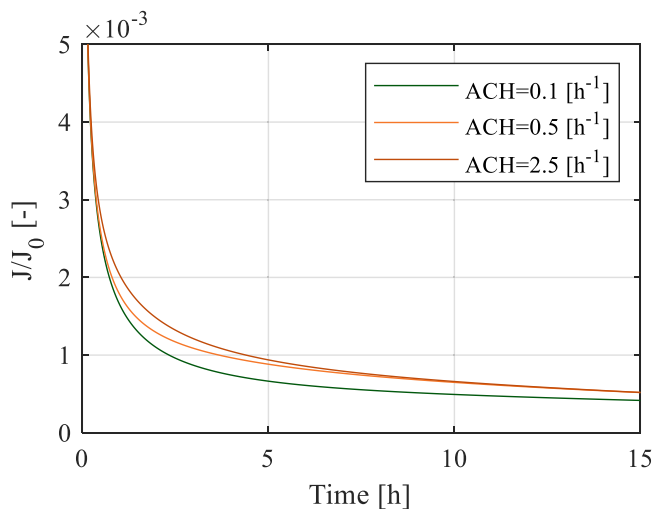


Fig. 8. Emission rates from one material for three cases with different ventilation.

there is no significant difference in emission rate if the room is ventilated at ventilation rates (ACH) of  $0.5 \text{ h}^{-1}$  or  $2.5 \text{ h}^{-1}$ . However, at ventilation rates lower than  $0.5 \text{ h}^{-1}$  the emission rate is noticeably affected. In this scenario, the ventilation rate is  $0.1 \text{ h}^{-1}$  which leads to a lower emission rate and longer time for depletion.

Our proposed method can also be used to study the depletion of VOC in a material at, for example, different ventilation rates. The total amount of VOC emitted from a material is given by integration over the timespan of interest. The solution is easily derived from the general solution, Eqs. (16) and (17), by division of the frequency parameter  $s$ .

As an example, we now calculate the depletion of VOC for our example at three different ventilation rates. The results from the simulations are presented in Fig. 9 (solid lines). Once again, the difference in depletion for the two higher ventilation rates ( $0.5 \text{ h}^{-1}$  and  $2.5 \text{ h}^{-1}$ ) is small while for ventilation rates much lower than  $0.5 \text{ h}^{-1}$  (in this case  $0.1 \text{ h}^{-1}$ ) the difference is much more significant. For example, a 50% depletion of all VOC in the material takes 3.1 h at  $\text{ACH} = 2.5 \text{ h}^{-1}$ , 3.7 h at  $\text{ACH} = 0.5 \text{ h}^{-1}$  and 18.9 h at  $\text{ACH} = 0.1 \text{ h}^{-1}$ , and similarly, a 75% depletion of all VOC in the materials takes 27.9 h at  $\text{ACH} = 2.5 \text{ h}^{-1}$ , 30.7 h at  $\text{ACH} = 0.5 \text{ h}^{-1}$ , and 45.2 h at  $\text{ACH} = 0.1 \text{ h}^{-1}$ .

As a comparison, in Fig. 9, we also show the concentration in the room (dashed lines) normalized against the initial material concentration. Here we see that concentrations are significantly lower at higher ventilation rates. This example illustrates that while increased

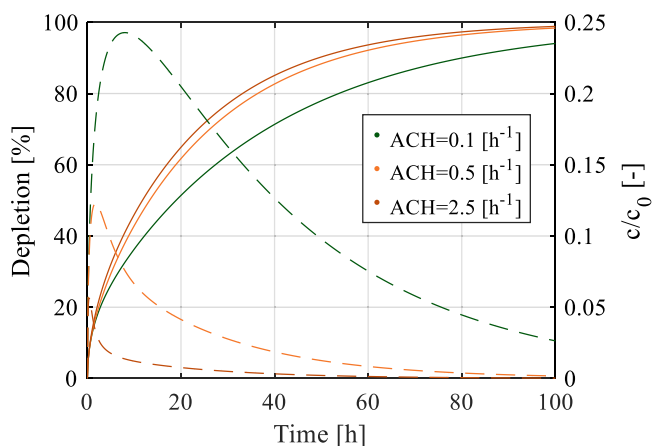


Fig. 9. Depletion of VOC for three cases with different ventilation rates together with room concentrations.

ventilation may not speed up the depletion of VOC from materials, increased ventilation may be necessary to keep concentrations at acceptable levels.

### 3. Results and discussion

#### 3.1. Example – meeting room

A typical office meeting room within the university premises is chosen as a reference for demonstrating the proposed model. The idea is to give a practical example of the usability of the model and show its ease of implementation. Initial concentrations for furniture, and diffusion- and partition coefficients are taken from the literature.

The furniture in the room is one large wooden table and ten wooden chairs. The ceiling has ceiling tiles, and the floor is vinyl. The innermost layer in three of the walls are painted gypsum boards and the fourth wall is made of glazing and has a glazed entrance door. The room has the following dimensions: length = 6.8 m, width = 3.9 m and height = 3.0 m. Table 2 shows a summary of the surfaces and their respective total emitting area.

Material properties such as diffusion coefficients, partition coefficients and initial concentrations are not found in abundance. For this example, material properties for emission of ethylbenzene are used because of its availability in literature [14,35,36]. However, initial concentrations for vinyl, gypsum boards and ceiling tiles are not found.

For ceiling tiles, we did not find studies confirming that they contain ethylbenzene and the initial concentration for the tiles is therefore assumed to be zero. However, both gypsum boards and vinyl flooring may emit ethylbenzene [37,38]. To make the example room more effective as a demonstration of the analytical model, the gypsums boards are given an initial concentration which is assumed to be in the same order of magnitude as the initial concentration in the wooden furniture.

Any material will eventually become empty of VOC if placed in a ventilated room and given enough time. A material may therefore contain any concentration between zero and its initial concentration shortly after it's been produced, depending on its history. To demonstrate the capability to handle sink-effects caused by empty materials the initial concentration of vinyl flooring is, in this example, assumed to be zero.

For a complete list of the input data for each material with corresponding references see Table 3. The material thickness for the table and the chairs is measured onsite while thickness of the floor, walls and ceiling tiles are based on typical thicknesses provided by producers.

Convective surface mass transfer coefficients vary with air velocity across the surface and with the type of VOC. Here, calculated using Sheerwood number as described by Huang and Haghighat [39]. The diffusion coefficient for Ethylbenzene in air is  $D = 7.5 \cdot 10^{-6} \text{ m}^2 \text{ s}^{-1}$  [40] and for air velocities ranging from  $0.01 \text{ ms}^{-1}$  to  $0.5 \text{ ms}^{-1}$  across the surface our calculations show that the mass transfer coefficients fall in the range of  $h = 0.0001 \text{ ms}^{-1}$  to  $h = 0.001 \text{ ms}^{-1}$ . For simplicity, the value  $h = 5.0 \cdot 10^{-4} \text{ ms}^{-1}$  is chosen for all the materials in this example.

The emission rates for each material, calculated with Eq. (16) and inverted with de Hoogs algorithm, are plotted in Fig. 10. Emission rates are normalized against the initial emission,  $J_0$ , given by Eq. (26). Negative values means that the material is absorbing (rather than emitting) VOC. In Fig. 10 the floor is initially acting as an absorbent,

Table 2 Summary of the emitting surfaces in the example room.

Part	Material	Area
Floor	Vinyl	26.5 m <sup>2</sup>
Walls	Gypsum	52.5 m <sup>2</sup>
Ceiling	Tiles	26.5 m <sup>2</sup>
Table	Wood	9.6 m <sup>2</sup>
Chairs	Wood	3.4 m <sup>2</sup>

**Table 3**  
Material properties and input data used in the simulations.

Ethylbenzene						
Part	Material	L [mm]	$c_0$ [ $\mu\text{g}/\text{m}^3$ ]	$D_m$ [ $\text{m}^2/\text{s}$ ]	$K_{ma}$ [-]	Reference
Floor	Vinyl	10	0	$1.6 \times 10^{-11}$	1920	[14]
Walls	Gypsum	15	$1e6^*$	$7.14e-10$	37.5	[35]
Ceiling	Tiles	15	0	$1.8e-9$	16	[35]
Table	Wood	10	$3.39e6$	$2.44e-10$	567	[36]
Chairs	Wood	10	$3.39e6$	$2.44e-10$	567	[36]

\* Assumed to be in the same order of magnitude as wood.

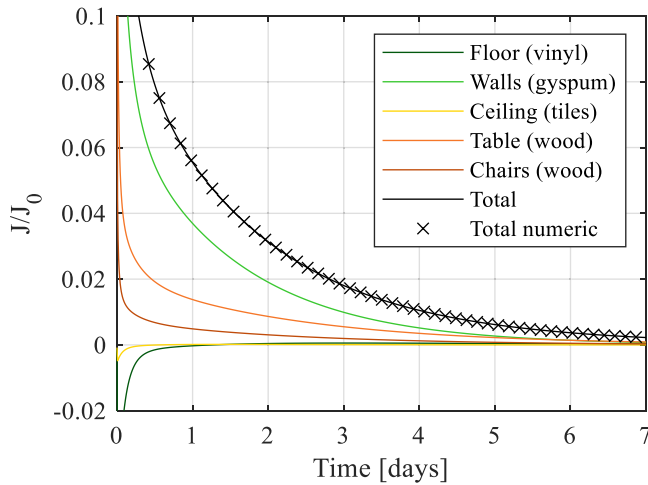


**Fig. 10.** Emission of ethylbenzene in the example room as a fraction of  $J_0$ .

taking up ethylbenzene from the room and emitting it later. The major contributor to the total emission is the gypsum walls.

### 3.2. Comparison with numerical solution

The numerical solution is found by discretizing each material in space and solving the change in concentration for each cell using finite differences. The result is then passed to an inbuilt ODE solver in MATLAB. Several solvers are tested and “ode15s” is found to be the most efficient. Fig. 10 show total emission calculated with the analytical model (black solid line) and total emission calculated with the numerical model (black crosses).

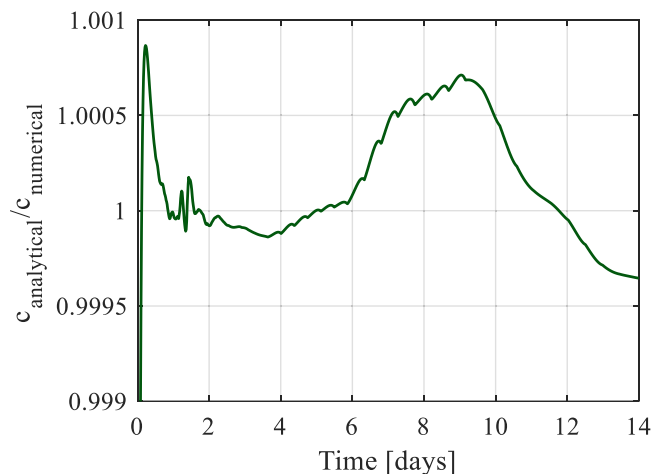


**Fig. 11.** The quotient between results from the analytical model and result from the numerical model.

In Fig. 11 the quotient between the results, indoor concentrations, from the analytical model and the results from the numerical model are plotted. Here, the value of one indicates a perfect match between the two solutions. As seen in the Fig. 11 there is close agreement between the two solutions. In addition, several comparisons were made between the numerical model and the analytical model with varying complexity and variations in input data. All these comparisons showed good agreement, like the above-mentioned example, between the two models.

In the example presented in Fig. 10, solving the Laplace inverse is about 10 times faster than solving it numerically. However, the computation time for the numerical solution is heavily dependent on the required fineness of the discretization in space. In this example 50 cells for each material are enough for the solution to converge. This was confirmed by calculating the average concentration for the entire simulation period using 25, 50, 75 and 100 cells respectively. For example, increasing the number of cells from 50 to 75 cells resulted in a difference in average concentration of less than 0.003 %.

However, when testing more complex material setups with larger variations in input data a higher number of cells is needed. In contrast, the computation time and accuracy for the analytical model is less affected by increased problem complexity.

Comparisons have also been made with analytical solutions found in the literature. These analytical solutions are usually solved by calculation of a convergent series; thus, the accuracy of these solutions is therefore dependent on the number of terms used in the series. For a large enough number of terms these analytical solutions are identical to the solutions given by the analytical model presented in this article. In such comparisons the major advantage of the proposed model lies in its flexibility and ease of implementation. For example, a direct comparison between the solution provided by Xiong et. al [9] and the proposed analytical model show identical results at comparable calculation times.

### 3.3. Emission and ventilation

In previous work a ventilation threshold of  $0.13 \text{ Ls}^{-1}\text{m}^{-2}$  ( $\text{m}^2$  emitting surface area) was proposed as an upper limit at which increased ventilation will have neglectable effect on emission rates [27]. Conclusions were drawn based on a model (equivalent to Eq. (26)) for one emitting material that does not include buffering capacity of the air in the room or the surface mass transfer. The time-constant (for one material) was introduced here to facilitate the analysis and relate material properties to the ventilation rate.

The time-constant together with the eerfc-function is useful for assessing the emission rates and room concentrations in relation to the ventilation rate and material properties. The eerfc-function is an approximation and limited by the assumptions of semi-infinite materials, neglectation of surface resistance and buffering capacity of the room. However, its simplicity makes it useful for drawing general conclusions. To better understand the impact of these simplifications (no buffering capacity in the air, no surface transfer resistance, and semi-infinite materials) we now define a new eerfc-function:

$$\text{eerfc}^* \left( \sqrt{t/t_c} \right) = \frac{c_a(t/t_c)}{c_0} \quad (40)$$

This expression,  $\text{eerfc}^*$ , does not have the above-mentioned simplifications and depends on several parameters. In contrast, the time-constant is the only parameter in the eerfc-function.

As a comparison, Fig. 12 shows the eerfc-function together with  $\text{eerfc}^*$  for the example room. The biggest difference between the two curves is seen in the beginning. The difference is caused by the effect of the buffering capacity of the room. The initial concentration for the air in the room is zero and since the buffering capacity in the eerfc-function is neglected the mass balance is reached instantly. With the  $\text{eerfc}^*$ -function the buffering capacity is accounted for, and the concentration in the room does not change instantly with changes in material emission rates. However, the typical time for the concentration in the room to

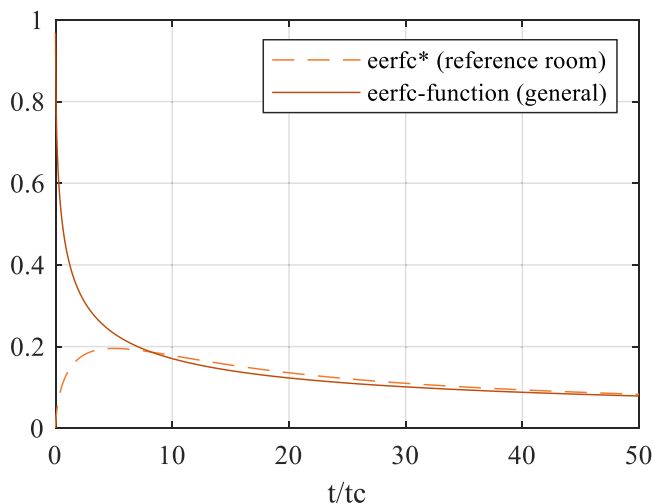


Fig. 12. The eercf-function compared with eercf\* calculated for the example room.

stabilize after a step-change is a couple of hours. Since the example room has a time-constant of about 20 min (calculated from Eq. (20)) the effect is visible even though several time-constants have passed. For larger time-constants, say of several hours, the effect of neglecting the buffering capacity would not be visible. It is important to note that, as discussed earlier, the eercf-function assumes a semi-infinite material and that these concentrations at longer times will be overestimated compared to the eercf\*.

The time-constant is room-dependent and decreases with increased ventilation. Typical values for time-constants have not been investigated. However, in the calculations performed in this work, typical values fall in the range of a couple of minutes to a couple of hours for ventilation rates of about 0.5 ACH.

A lower concentration in the room can be achieved either by “waiting” to let more emissions diffuse through the material and exit the room through ventilation or by increasing the ventilation to achieve a lower time-constant. However, the effect of increased ventilation on the concentration is stronger at smaller times because of higher concentrations near the surface that are easily emitted. The near surface emissions are hindered more by convection than by the diffusivity of the material. As the near surface concentrations start to decrease emissions need to diffuse from deeper inside the material before they are emitted to the room. At this stage, the diffusivity is more decisive for the emission rates.

The time-constant describes the relation between diffusivity and ventilation in terms of time. For example, to half the time-constant we can increase the ventilation by 41 % ( $\sqrt{2} \approx 1.41$ ), see Eq. (20), which means that the concentration found at 10 time-constants now equals the concentration found at 20 time-constants, see Fig. 12. However, the slope of the eercf-function is steeper at small  $t/t_c$  and therefore a higher ventilation (smaller time-constant) has a larger effect on the concentration at small times.

Since the emission rate is directly proportional to the ventilation times the eercf-function ( $J \propto Ra \bullet eercf$ ) the effect of higher ventilation can be estimated easily. For example, let us consider the emission rate at  $t/t_c = 10$ . The relative emission rate is then  $J \propto 1 \bullet eercf(10) = 0.171$ . With a ventilation rate that is 44 % higher the time-constant is halved, and the new relative emission rate is  $J \propto 1.44 \bullet eercf(20) = 0.174$ , which is a difference in emission rate of 1.8 % compared to the lower ventilation rate. The relative difference in emission rates between a higher and a lower ventilation rate decreases with time.

In terms of time, if taking the reference room as an example, 10 time-constants are 3 h and 20 min ( $t_c = 20$  min). The indoor concentration after 6 h and 40 min with normal ventilation will therefore be the same

as after 3 h and 20 min with doubled ventilation. A couple of hours of extra time is usually neglectable in the context of a new building.

This can be used as a strategy for determining the ventilation rate. If we assume that the goal is to reduce the concentration in the room by about 90 % from its initial value (the total initial concentration) it takes  $t/t_c = 40$  (see Fig. 12). With a time-constant of 20 min this takes 13 h and 20 min. If the time is too long the ventilation rate can be increased by 44 % and it will instead take 6 h and 40 min to reduce initial concentration by 90 %.

### 3.4. Sensitivity analysis

In the comparison presented in Fig. 11 the computation time for the analytical model is 10 times faster than the numerical solution. In addition, the difference in computation time between the analytical model and the numerical model tends to become larger with increased problem complexity and larger variations in input data. Also, throughout this work there has been no need for fine tuning the tolerance parameters in de Hoog’s algorithm, while the numerical model needed several rounds of mesh refinement to find a converged solution.

There is a shortage in available material properties ( $D_m$  and  $K_{ma}$ ) for material-VOC combinations. In addition, material properties may vary significantly between materials of the same type. One way of handling this uncertainty is the use of probability distribution functions as input parameters rather than fixed values together with repeated simulations (Monte Carlo simulations) where the obtained results are given as probability distributions. Unfortunately, for models where the evaluation time is significant, such simulations can become quite time consuming. The proposed analytical model is especially well-suited for Monte Carlo simulation given the above presented advantages of robustness and short evaluation times.

As an example, we will now use Monte Carlo simulations to compare the general eercf-function

with the eercf\*-function as defined by Eq. (40). In this example we make computations for the example room but at each iteration the initial concentration, the partition coefficient and the diffusion coefficient are chosen randomly within the following intervals:  $0 \leq c_0 \leq 10^6$ ,  $10 \leq K_{ma} \leq 2000$  and  $10^{-11} \leq D_m \leq 10^{-9}$ . The intervals are chosen based on the lowest and highest values found in Table 3. All the simulations are made at  $t/t_c = 10$  and results are presented as the quotient between eercf\* and the eercf-function.

In Fig. 13 probability (top) and cumulative distribution (bottom) is shown for the Monte Carlo simulation with 10000 iterations. Most of the results have a lower value than one which means that the eercf-function, in most cases, leads to overestimation of the room concentration. In this example the eercf-function underestimates the results in 2.5 % of the cases, where the largest underestimation found within those 2.5 % is about 7 % lower than the value for eercf\*. The probability distribution is quite even around 0.02 for all bins between zero and one. The main explanation is that the concentrations reduce more quickly as the materials become more depleted ( $L^2/D_m < t$ ). To illustrate this the Monte Carlo simulation is repeated with the same setup except from material thicknesses which are given an infinite thickness. The resulting probability (top) and cumulative distribution (bottom) is seen in Fig. 14. Here the overestimation is smaller, and all values fall between 0.95 and 1.05.

## 4. Future work

The solutions presented in this paper are valid for any number of materials and account for material diffusion, surface transport and room storage capacity. In addition, the presented method is flexible and can be used to derive solutions for different setups of rooms with emitting or absorbing materials. In future work the method will be used to investigate emissions from materials built into the construction and how built in materials affect long-term emission decline. Also, more work will be

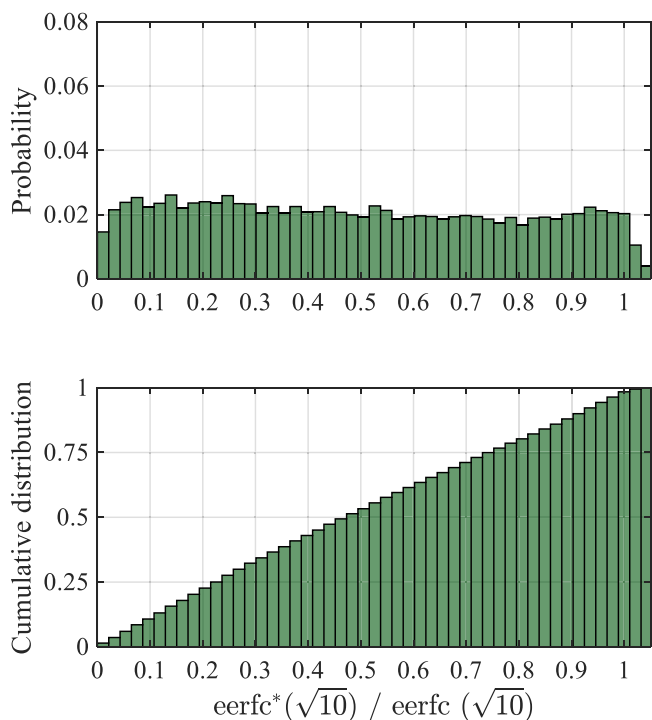


Fig. 13. Results from Monte Carlo simulations with material thicknesses in accordance with the example room. Top: probability distribution. Bottom: cumulative distribution.

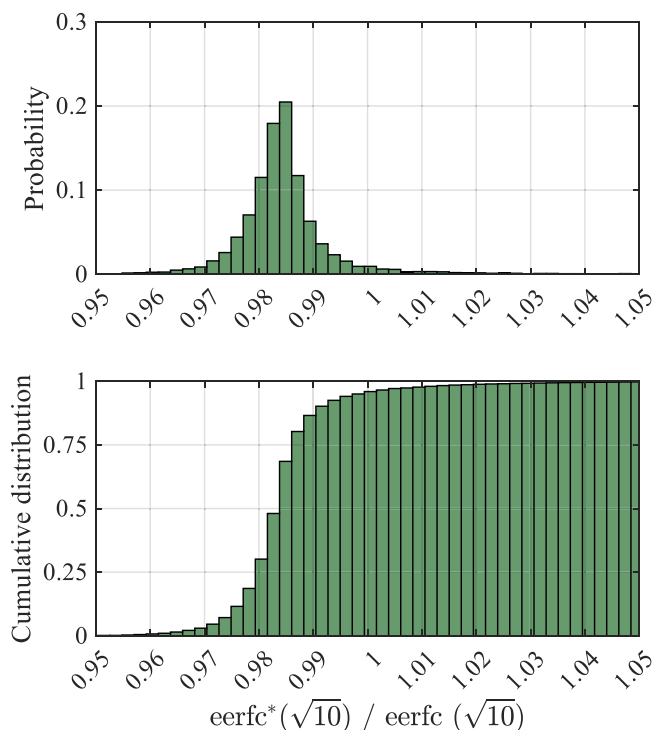


Fig. 14. Results from Monte Carlo simulations with semi-infinite materials. Top: probability distribution. Bottom: cumulative distribution.

put into emission modeling on a building scale. By utilizing the possibility of sensitivity analysis with Monte Carlo simulations new insights can be gained regarding timescales and distribution of emissions and concentrations in whole buildings.

## 5. Conclusions

The proposed method, based on Laplace Networks, is both efficient and flexible for analyzing and predicting VOC emissions from materials. As demonstrated in this work, it enables precise predictions while also providing insights into timescales and model parameters through, for example, asymptotic analysis. The flexibility and short computation times make the model particularly useful for sensitivity analysis. For example, capturing and understanding the impact of uncertainty in input data on room concentrations and emission rates.

The relation between emission rates and ventilation is of particular relevance since, in new buildings, ventilation systems are often run at enhanced levels under the assumption that this accelerates VOC depletion from building materials with increased energy usage as a direct consequence. Our analysis reveals that increasing ventilation beyond normal levels has a negligible impact on the emission rate for the simulated materials. This underscores the need to revise strategies for managing VOC emissions in new buildings and to develop more effective approaches for improving indoor air quality in new buildings.

### CRediT authorship contribution statement

**Carl-Eric Hagentoft:** Writing – review & editing, Writing – original draft, Methodology, Formal analysis, Conceptualization. **Fredrik Domhagen:** Writing – review & editing, Writing – original draft, Methodology, Investigation, Formal analysis, Conceptualization.

### Declaration of Competing Interest

The authors declare that they have no known competing financial interests or personal relationships that could have appeared to influence the work reported in this article.

### Acknowledgements

This work was supported and funded by Chalmers University of Technology.

### References

- [1] M.T. Baeza Romero, M.R. Dudzinska, M. Amouei Torkmahalleh, N. Barros, A. M. Coggins, D.G. Ruzgar, I. Kildsgaard, M. Naseri, L. Rong, J. Saffell, A.M. Scutaru, A. Staszowska, A review of critical residential buildings parameters and activities when investigating indoor air quality and pollutants, *Indoor Air* 32 (2022), <https://doi.org/10.1111/ina.13144>.
- [2] S. Vardoulakis, E. Giagloglou, S. Steinle, A. Davis, A. Sleenwenhoeck, K.S. Galea, K. Dixon, J.O. Crawford, Indoor exposure to selected air pollutants in the home environment: a systematic review, *Int. J. Environ. Res. Public Health* 17 (2020) 8972, <https://doi.org/10.3390/ijerph17238972>.
- [3] F. Felgueiras, Z. Mourão, A. Moreira, M.F. Gabriel, Indoor environmental quality in offices and risk of health and productivity complaints at work: a literature review, *J. Hazard. Mater. Adv.* 10 (2023) 100314, <https://doi.org/10.1016/j.hazadv.2023.100314>.
- [4] D.A. Missia, E. Demetriou, N. Michael, E.I. Tolis, J.G. Bartzis, Indoor exposure from building materials: a field study, *Atmos. Environ.* 44 (2010) 4388–4395, <https://doi.org/10.1016/j.atmosenv.2010.07.049>.
- [5] Y.M. Kim, S. Harrad, R.M. Harrison, Concentrations and sources of VOCs in urban domestic and public microenvironments, *Environ. Sci. Technol.* 35 (2001) 997–1004, <https://doi.org/10.1021/es000192y>.
- [6] D. Panagiotaras, Comprehensive experience for indoor air quality assessment: a review on the determination of volatile organic compounds (VOCs), *J. Phys. Chem. AMP Biophys.* 4 (2014), <https://doi.org/10.4172/2161-0398.1000159>.
- [7] S.B. Holøs, A. Yang, M. Lind, K. Thunshelle, P. Schild, M. Mysen, VOC emission rates in newly built and renovated buildings, and the influence of ventilation – a review and meta-analysis, *Int. J. Vent.* 18 (2018) 153–166, <https://doi.org/10.1080/14733315.2018.1435026>.
- [8] Z. Liu, W. Ye, J.C. Little, Predicting emissions of volatile and semivolatile organic compounds from building materials: a review, *Build. Environ.* 64 (2013) 7–25, <https://doi.org/10.1016/j.buildenv.2013.02.012>.
- [9] J. Xiong, C. Liu, Y. Zhang, A general analytical model for formaldehyde and VOC emission/sorption in single-layer building materials and its application in determining the characteristic parameters, *Atmos. Environ.* 47 (2012) 288–294, <https://doi.org/10.1016/j.atmosenv.2011.10.063>.

- [10] H. Karlsson, A.S. Kalagasidis, C.-E. Hagentoft, Development of a modular toolbox in Simulink for dynamic simulations of VOC-concentration in indoor air, International Building Simulation Conference, Montreal (2005).
- [11] M. Guo, W. Yu, S. Zhang, H. Wang, S. Wei, A numerical model predicting indoor volatile organic compound volatile organic compounds emissions from multiple building materials, *Environ. Sci. Pollut. Res.* 27 (2020) 587–596.
- [12] J. Xiong, S. Huang, Y. Zhang, A novel method for measuring the diffusion, partition and convective mass transfer coefficients of formaldehyde and VOC in building materials, *PLOS One* 7 (2012) e49342.
- [13] J. Xiong, Y. Yao, Y. Zhang, C-history method: rapid measurement of the initial emittable concentration, diffusion and partition coefficients for formaldehyde and VOCs in building materials, *Environ. Sci. Technol.* 45 (2011) 3584–3590.
- [14] A. Bodalal, J.S. Zhang, E.G. Plett, A method for measuring internal diffusion and equilibrium partition coefficients of volatile organic compounds for building materials, *Build. Environ.* 35 (2000) 101–110, [https://doi.org/10.1016/S0360-1323\(99\)00005-0](https://doi.org/10.1016/S0360-1323(99)00005-0).
- [15] H.S. Carslaw, J.C. Jaeger, *Conduction of Heat in Solids*, Oxford University Press, 1959.
- [16] G. Jóhannesson, *Active Heat Capacity: Models and Parameters for the Thermal Performance of Buildings*, Division of Building Physics, 1981.
- [17] C.-E. Hagentoft, S. Pallin, Thermal step response of N-Layer composite Walls—Accurate approximative formulas, *J. Heat. Transf.* 142 (2020), <https://doi.org/10.1115/1.4045642>.
- [18] X. Yang, Q. Chen, J.S. Zhang, R. Magee, J. Zeng, C.Y. Shaw, Numerical simulation of VOC emissions from dry materials, *Build. Environ.* 36 (2001) 1099–1107.
- [19] Y. Xu, Y. Zhang, A general model for analyzing single surface VOC emission characteristics from building materials and its application, *Atmos. Environ.* 38 (2004) 113–119.
- [20] N. Liu, X. Zhang, L. Wang, K. Liang, Y. Zhang, J. Cao, Early-stage emissions of formaldehyde and volatile organic compounds from building materials: model development, evaluation, and applications, *Environ. Sci. Technol.* 56 (2022) 14680–14689.
- [21] H. Chen, N. Liu, J. Guo, L. Wang, Y. Zhang, J. Wei, Y. Xu, Y. Cao, Y. Zhang, Two-parameter C-history method: a fast and accurate method for determining the characteristic parameters of formaldehyde/VOC early-stage emissions from building materials, *Sci. Total Environ.* 946 (2024) 174218, <https://doi.org/10.1016/J.SCITOTENV.2024.174218>.
- [22] Y. Zhang, N. Xu, J. Liu, Z. Guo, H. Guan, Y. Bai, A multisource mass transfer model for simulating VOC emissions from paints, *Sci. Total Environ.* 902 (2023), <https://doi.org/10.1016/J.SCITOTENV.2023.165945>.
- [23] F. Haghighat, H. Huang, Integrated IAQ model for prediction of VOC emissions from building material, *Build. Environ.* 38 (2003) 1007–1017, [https://doi.org/10.1016/S0360-1323\(03\)00064-7](https://doi.org/10.1016/S0360-1323(03)00064-7).
- [24] L.Z. Zhang, J.L. Niu, Modeling VOCs emissions in a room with a single-zone multi-component multi-layer technique, *Build. Environ.* 39 (2004) 523–531, <https://doi.org/10.1016/j.buildenv.2003.10.005>.
- [25] B. Deng, B. Yu, C.N. Kim, An analytical solution for VOCs emission from multiple sources/sinks in buildings, *Sci. Bull.* 53 (2008) 1100–1106, <https://doi.org/10.1007/s11434-008-0015-0>.
- [26] B. Deng, S. Tang, J.T. Kim, C.N. Kim, Numerical modeling of volatile organic compound emissions from multi-layer dry building materials, *Korean J. Chem. Eng.* 27 (2010) 1049–1055, <https://doi.org/10.1007/s11814-010-0208-5>.
- [27] F. Domhagen, S. Langer, A. Sasic Kalagasidis, Theoretical threshold for estimating the impact of ventilation on Materials' emissions, *Environ. Sci. Technol.* 58 (2024) 5058–5067, <https://doi.org/10.1021/acs.est.3c09815>.
- [28] C.-E. Hagentoft, *Introduction to Building Physics*, Studentlitteratur, Lund, 2001.
- [29] M. Cohen Alan, *Numerical Methods for Laplace Transform Inversion*, Springer-Verlag, New York Inc, 2007.
- [30] K.L. Kuhlman, Review of inverse laplace transform algorithms for Laplace-space numerical approaches, *Numer. Algorithms* 63 (2012) 339–355, <https://doi.org/10.1007/s11075-012-9625-3>.
- [31] F.R. de Hoog, J.H. Knight, A.N. Stokes, An improved method for numerical inversion of laplace transforms, *SIAM J. Sci. Stat. Comput.* 3 (1982) 357–366, <https://doi.org/10.1137/0903022>.
- [32] T mpmath development team, mpmath: a Python library for arbitrary-precision floating-point arithmetic (version 1.3.0), (2023).
- [33] K. Hollenbeck, INVLAP. M.: A matlab function for numerical inversion of Laplace transforms by the de Hoog algorithm, (<Http://Www>). Isva. Dtu. Dk/Staff/Karl/Invlap. Htm (1998).
- [34] W.I. Well, *WELL Building Standard*, International Well Building Institute, New York, NY, USA, 2020.
- [35] J. Zhang, J.S. Zhang, Q. Chen, Effects of environmental conditions on the sorption of VOCs on building materials-part II: model evaluation (RP-1097), *Trans. Am. Soc. Heat. Refrig. Air Cond. Eng.* 109 (2003) 167–178.
- [36] Y. Yao, J. Xiong, W. Liu, J. Mo, Y. Zhang, Determination of the equivalent emission parameters of wood-based furniture by applying C-history method, *Atmos. Environ.* 45 (2011) 5602–5611, <https://doi.org/10.1016/j.atmosenv.2011.04.033>.
- [37] Y.-H. Cheng, C.-C. Lin, S.-C. Hsu, Comparison of conventional and Green building materials in respect of VOC emissions and ozone impact on secondary carbonyl emissions, *Build. Environ.* 87 (2015) 274–282, <https://doi.org/10.1016/j.buildenv.2014.12.025>.
- [38] O. Wilke, O. Jann, D. Brodner, VOC- and SVOC-emissions from adhesives, floor coverings and complete floor structures, *Indoor Air* 14 (2004) 98–107, <https://doi.org/10.1111/j.1600-0668.2004.00314.x>.
- [39] H. Huang, F. Haghighat, Modelling of volatile organic compounds emission from dry building materials, *Build. Environ.* 37 (2002) 1127–1138, [https://doi.org/10.1016/S0360-1323\(01\)00089-0](https://doi.org/10.1016/S0360-1323(01)00089-0).
- [40] R.K. Rowe, T. Mukunoki, H.P. Sangam, Benzene, toluene, ethylbenzene, m & p-Xylene, o-Xylene diffusion and sorption for a geosynthetic clay liner at two temperatures, *J. Geotech. Geoenviron. Eng.* 131 (2005) 1211–1221, [https://doi.org/10.1061/\(asce\)1090-0241\(2005\)131:10\(1211\)](https://doi.org/10.1061/(asce)1090-0241(2005)131:10(1211)).